Available online at www.sciencedirect.com

ScienceDirect

www.elsevier.com/locate/matchar

# Extrusion textures in Al, 6061 alloy and 6061/$SiC_p$ nanocomposites

X. Jiang[a,1], M. Galano[a,*], F. Audebert[a,b,c,2]

[a]Department of Materials, University of Oxford, Parks Road, OX1 3PH Oxford, UK
[b]Advanced Materials Group, Facultad de Ingeniería, Universidad de Buenos Aires, Paseo Colón 850, Buenos Aires 1063, Argentina
[c]Department of Mechanical Engineering and Mathematical Sciences, Oxford Brookes University, Wheatley Campus, OX33 1HX Oxford, UK

ARTICLE DATA

*Article history:*
Received 19 April 2013
Received in revised form 13 November 2013
Accepted 23 November 2013

*Keywords:*
Metal matrix composites
Al alloys
Extrusion
Texture
ODF
EBSD

ABSTRACT

The 6061 alloy matrix composites reinforced with 10 wt.% and 15 wt.% of SiC nanoparticles with an average diameter of ~500 nm were hot extruded in strip shape from ball milled powders. The microstructures and textures of the hot extruded nanocomposites have been investigated by means of three dimensional orientation distribution functions and electron backscatter diffraction (EBSD) techniques. Pure Al and 6061 alloy extruded strips from atomised powders have been produced for comparison purposes. The results show that the non-deformable SiC particulates have a strong influence on the formation of extrusion textures in the matrix. Pure Al and 6061 alloy develop a typical β fibre texture after extrusion in strip shape. For 6061/$SiC_p$ nanocomposites, the intensities of major texture components decrease with increasing amount of SiC particles. The total intensities of Brass, Dillamore and S components have decreased by 19% for 6061/10 wt.% $SiC_p$ and 40% for 6061/15 wt.% $SiC_p$ composites when compared with the 6061 alloy. EBSD analysis on local grain orientations shows limited Al grain rotations in SiC rich zones and decreased texture intensities.



## 1. Introduction

Particulate reinforced aluminium alloy composites are attractive materials for automotive, aeronautic and aerospace applications due to their low density, high Young's modulus and strength and high wear resistance [1]. These aluminium alloy matrix composites can be produced by powder metallurgy routes followed by secondary forming processes, such as extrusion and rolling [2].

Investigations on the development of crystallographic texture during extrusion and rolling of aluminium alloy composites have been carried out since the matrix texture components produce anisotropy in the mechanical properties of the composites [3]. Although there are many evidences that the addition of reinforcement particles alters the texture evolution of the alloy matrix, this effect has not been understood thoroughly yet.

The rolling texture of aluminium alloys has been extensively studied and is well known [4–7]. It is mostly represented by continuous tubes or fibres of orientations limited to a single degree of rotational freedom about a fixed axis [4] in three dimensional Euler space. For cold rolled aluminium, the texture mainly consists of α fibre which goes from Goss component ({1 1 0} <0 0 1>) to Brass component ({1 1 0} <1 1 2>) and β fibre running from Brass component to Copper component ({1 1 2} <1 1 1>) through S component ({1 2 3} <6 3

* *Corresponding author*. Tel.: +44 1865 273731; fax: +44 1865 273789.
E-mail addresses: xia.jiang@materials.ox.ac.uk (X. Jiang), marina.galano@materials.ox.ac.uk (M. Galano), fernando.audebert@materials.ox.ac.uk (F. Audebert).
[1] Tel.: +44 1865 273776.
[2] Tel.: +44 1865 424522.

1044-5803/$ – see front matter © 2013 Elsevier Inc. All rights reserved.
http://dx.doi.org/10.1016/j.matchar.2013.11.009

4>) [5]. For hot rolled aluminium alloys, the texture components are similar to cold rolled aluminium alloys, however usually showing increased overall texture intensity, a large increase of Brass component and the presence of Cube ({0 0 1} <1 0 0>) or near Cube component when certain temperature has been reached [8–10].

However, the deformation texture of aluminium alloy composites has not yet been studied quantitatively. Humphreys et al. [11] investigated the effect of 7 μm SiC particles on the hot rolling texture of aluminium and found out that the addition of 10 vol.% SiC particles has led to a considerable reduction in the intensities of the main textures. Jensen et al. [12] studied the effect of different particle sizes on the evolution of texture components and determined a critical particle size of around 0.1 μm, below which the intensities of texture were higher than unreinforced materials. Other authors [13] found out that the texture of aluminium alloy composites was also related to particle concentrations and particle shapes. In addition, the authors noticed that despite of the increasing number of texture studies for aluminium alloy composites after secondary forming processes, most researchers focus on the texture evolution after cold or hot rolling while very limited number of papers report the evolution of texture in hot extruded aluminium alloy based composites [14]. Even fewer papers report texture studies for aluminium alloys reinforced with nanosized particles in hot extruded conditions. He et al. [15] investigated the texture development in aluminium reinforced with SiC particles of different sizes (25 nm, 150 nm and 3.5 μm) and different volume fractions after hot extrusion into rods and found out that the texture intensities of Al matrix tend to decrease for the aluminium matrix composite (AlMC) reinforced with 3.5 μm SiC particles while increase for nanosize reinforced AlMCs. However, no information is available on texture studies of nanosize reinforced aluminium alloy composites after extrusion in strip shape. Compared with the most frequently used rod extrusion, flat extrusion enables the formation of Al sheets or strips in only one forming step. Also it makes the subsequent process, such as rolling, much easier to perform.

In order to understand the effect of hot extrusion and nanosize reinforcements to the texture development of aluminium alloy matrix composites, in the present work, the 6061 aluminium alloy was reinforced with different weight fractions of 500 nm SiC particles by powder metallurgy routes and followed by hot extrusion into strip shape. The texture development in the composites after extrusion was compared with the texture in an unreinforced alloy. Both the orientation density functions (ODF) and the electron backscatter diffraction (EBSD) techniques were applied to fully understand texture evolution in macro- and micro-scales.

## 2. Experimental

The 6061 alloy matrix composites reinforced with 10 wt.% and 15 wt.% of SiC nanoparticles with an average diameter of around 500 nm were received from an industrial collaborator in the form of billets. The billets were fabricated by high energy ball milling followed by solid state compaction and hipping. For comparison purposes, 6061 alloy atomised powder of an average size of 10 μm and pure aluminium atomised powder of an average size of 4 μm were cold compacted into 30 mm diameter billets with a load of 350 kN. All the billets were extruded at 375 °C to obtain strips of rectangle cross section with a thickness of 6 mm and width of 20 mm. The extrusion ratio (ER) was 6:1 which produced a true strain of 1.8 $\left(\varepsilon = \ln\left(\frac{A_{\text{initial}}}{A_{\text{final}}}\right)\right)$. Microstructural characterization of as-received and as-extruded materials was carried out in a JSM-6300 scanning electron microscope (SEM). As-extruded samples were cut from strip sections parallel to the extrusion direction.

The crystallographic texture of as-extruded samples was measured by X-ray diffraction on a Philips X'pert MRD system. All samples used for texture analysis were taken from the intermediate section of the strips. In order to maximise the reflexion area the measurements were carried out on the ED–TD plane (ED: extrusion direction; TD: transverse direction). Four incomplete pole figures {1 1 1}, {2 0 0}, {2 2 0} and {3 1 1} were measured up to a maximum tilt angle of 85° by the Schulz back-reflection method using Cu–Kα radiation. Orientation distribution functions (ODFs) were then calculated from the pole figures after background and defocusing corrections by means of Matlab software toolbox MTEX [16]. ODFs were presented in plots in constant $\varphi_2$ sections with iso-intensity contours in Euler space. A three dimensional Euler space is defined by Euler angles $\varphi_1$, $\Phi$, and $\varphi_2$ which describe the three rotations to overlap the sample reference frame with the crystal reference frame. Although every orientation can be precisely represented by a point in Euler space, sometimes it is difficult to interpret a 3D graph. Hence, ODF, a 2D representation of Euler space constructed by dividing into slices at constant intervals, is commonly used for texture analysis [4].

The electron backscatter diffraction (EBSD) technique was used to investigate the microscopic texture of as-received and as-extruded samples. EBSD sample preparation for samples with multiple phases is always quite difficult due to surface relief, especially for areas in the vicinity of secondary particles. Different polishing techniques have been tried out; the technique that gave the best pattern was to perform the final surface treatment in a Precision Ion Polishing System (PIPS) Gatan Model 691 after standard mechanical grinding and polishing. $Ar^+$ ions polished the surface of a rotating sample at a very low bombardment angle (1°) at a voltage of 4 kV, lowering the height differences between the matrix and SiC particles, and greatly reducing the surface roughness in the Al/SiC interface [17]. For as-received 6061Al/$SiC_p$ billets, EBSD scans were conducted on the longitudinal planes of the billets by means of automated acquisition and indexing of Kikuchi patterns in a TSL system interfaced to a JSM-6300/JSM-840A SEM with a scan step of 100–200 nm. For a better comparison of the texture results, EBSD scans on the as-extruded samples were performed at the same areas (ED–TD planes) used for crystallographic texture analysis carried out by X-ray diffraction.

## 3. Results and Discussions

### 3.1. *Microstructure*

Fig. 1 shows secondary electron images of as-received and as-extruded 6061/$SiC_p$ nanocomposites. It can be seen from

Fig. 1(a) and (b) that the SiC particles are not homogeneously distributed in the as-received billets. There are some areas free of SiC particles. After extrusion, those areas are observed as particle free bands with a width of 5–10 μm along the extrusion direction, leading to a macroscopic anisotropy in the extruded strips. This banded structure, with particle free zones, has been observed previously for this type of composites [2,18–21]. Sun et al. [20] studied the microstructure of Al/$SiC_p$ composites after hot extrusion with different extrusion ratios ranging from 11:1 to 39:1 and found out that there were many dark bands (SiC rich areas) and bright belts parallel to the extrusion direction. The boundaries between bright and dark bands became diluted with increasing extrusion ratio. Similar results were also reported by Wang et al. [21] indicating a less uniform distribution of SiC particles when the extrusion ratio was 5:1 and the particle distribution was significantly improved when the extrusion ratio increased to 12:1. Therefore, the banded structure observed in the present work after extrusion, with a ER of 6:1 (see Fig. 1(c) and (d)) is in agreement with those results found by Sun et al. [20] and Wang et al. [21].

Other authors [2,19,21] have analysed the effect of the extrusion temperature on the microstructure of Al alloy matrix composites and found out a more uniform particle distribution with increasing extrusion temperature up to a certain value. If the temperature is not high enough, it cannot facilitate the flow of the matrix alloy under the applied stress resulting in a non-homogeneous distribution of the particles. If extrusions are carried out at a relatively high temperature, partial melting of the matrix alloy at the grain boundaries happens causing the particles to get suspended in the melt matrix near the grain boundaries [2]. In the present work, both composites were extruded at 375 °C which is lower than the average extrusion temperature (~500 °C) for 6061 alloy matrix composites reinforced with similar amount of SiC particles reported in the literature [19]. The combined effects of a small extrusion ratio and a low extrusion temperature will certainly lead to a non-sufficient flow of the matrix alloy, resulting in a non-uniform distribution of SiC particles among the Al alloy matrix leading to a banded structure.

Extrusion is always reported to effectively decrease the number of pores and improve the interfacial bonding strength between matrix and reinforcement particles [2,22]. Despite the reduced amount of porosity compared to as-received samples, a certain amount of voids remained after the extrusion, as can be observed in Fig. 1(c) and (d) (see arrows). A higher extrusion ratio and temperature would facilitate the flow of the matrix alloy filling the voids and break up the

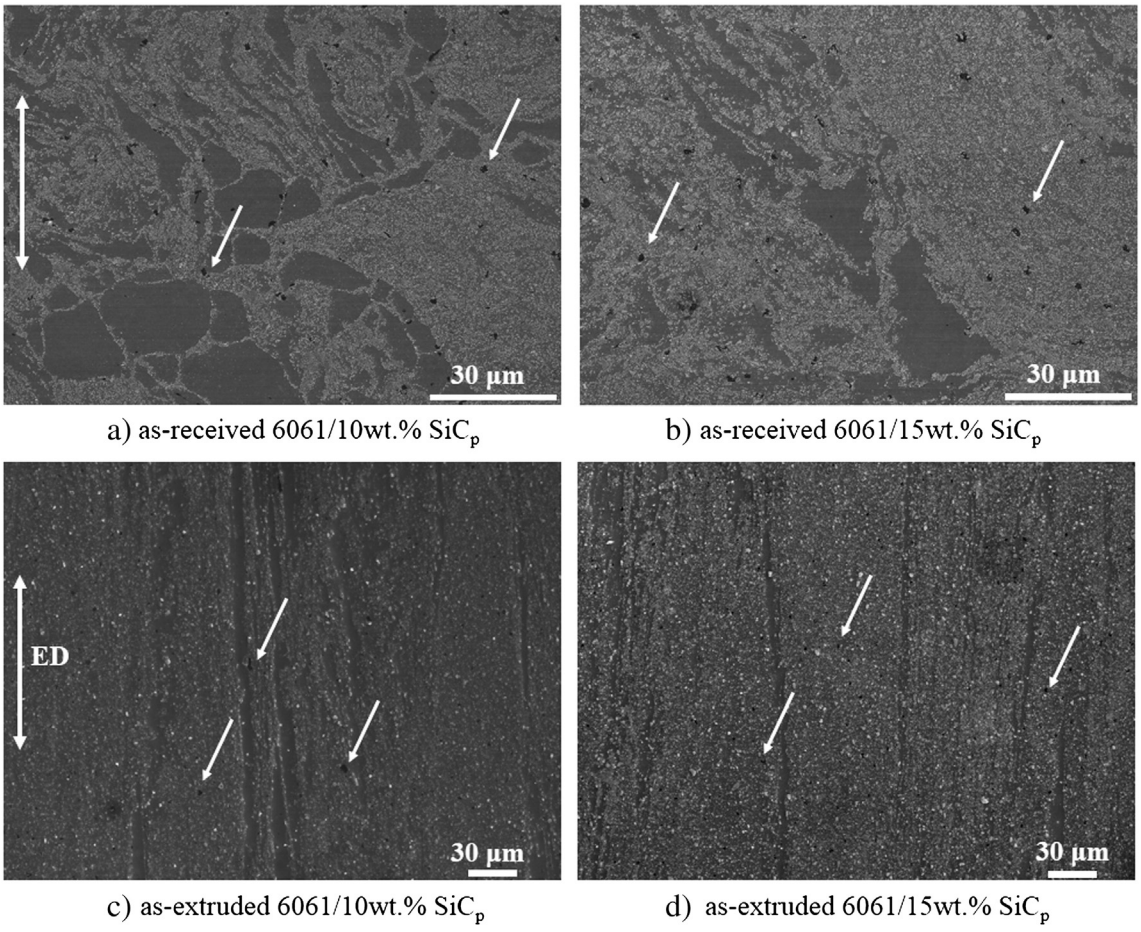


**Figure 1 – Secondary electron images of as-received and as-extruded 6061/$SiC_p$ nanocomposites. Arrows indicate porosity.**

oxide layers on the surface of Al alloy powders, enhancing the bonding strength between powder particles. However, high temperature and extrusion ratio can lead to dynamic recrystallization losing the strength gained by work hardening during the extrusion process [23].

### 3.2. *Crystallographic Texture Study by ODFs*

Fig. 2 shows the ODFs of pure Al, 6061 alloy and 6061/$SiC_p$ nanocomposites after extrusion at 375 °C. It can be seen that the texture can be described by a β′ fibre which is close to the typical β fibre from cold rolled aluminium alloys. For pure Al, the β′ fibre mainly contains the components of B′—{0 10 10} <10 7 7> ($\varphi_1$ = 45°, Φ = 45°, $\varphi_2$ = 0°), S′—{2 2 5} <10 9 7> ($\varphi_1$ = 40°, Φ = 70°, $\varphi_2$ = 20°) and D′—{2 5 10} <10 7 6> ($\varphi_1$ = 65°, Φ = 30°, $\varphi_2$ = 65°). For 6061 alloy, the β′ fibre contains the orientations of B′—{0 8 10} <10 6 5> ($\varphi_1$ = 40°, Φ = 40°, $\varphi_2$ = 0°), S′—{2 3 5} <10 6 7> ($\varphi_1$ = 30°, Φ = 60°, $\varphi_2$ = 20°) and D′—{3 6 10} <10 6 7> ($\varphi_1$ = 60°, Φ = 35°, $\varphi_2$ = 65°). All of the components are totally different from the typical axial fibre textures obtained in aluminium alloys after extrusion into rods [19,24], however, very similar to the results reported for aluminium alloys extruded in strip shape [25,26].

The β′ fibre textures obtained are quite close to the major orientations of typical textures observed in cold and hot rolled aluminium, which are Brass component ({0 1 1} <2 1 1>), $S_1$ component ({1 2 4} <2 1 1>) and Dillamore component ({4 4 11} <11 11 8>) [4]. In the present work, the extruded specimens have been compressed in the normal directions of the strips and elongated along the extrusion directions. Hence, it is not surprising that a β′ fibre texture has formed after extrusion since the deformation state during extrusion of a circular bar to a flat strip is very similar to the plane strain hot rolling process [26]. It is suggested that with further deformations, the texture components for pure Al and 6061 alloy will gradually rotate to those standard orientations and develop a typical β fibre texture in the end.

For 6061/$SiC_p$ nanocomposites, the texture components are quite similar with each other. Besides the random texture, there are three moderate strong texture components, which are B′—{0 10 10} <5 3 3> ($\varphi_1$ = 40°, Φ = 45°, $\varphi_2$ = 0°) with a scatter along α fibre, S′—{2 2 5} <10 9 7> ($\varphi_1$ = 40°, Φ = 70°, $\varphi_2$ = 20°) and D′—{2 5 10} <10 7 6> ($\varphi_1$ = 65°, Φ = 30°, $\varphi_2$ = 65°), and a weak scatter of the cube orientation. The three moderate strong texture components are near the typical texture components in both cold and hot rolled aluminium within several degrees' tolerance.

Comparing the main texture components in the four as-extruded samples, the main textures in 6061/$SiC_p$ nanocomposites are weaker than those in pure Al and 6061 alloy. Fig. 3 shows the maximum texture intensities for the three dominant texture components near Brass (B′), Dillamore (D′) and $S_1$ (S′) positions. From the figure, it can be seen that for all the as-extruded samples, the texture intensities near Brass component are higher compared to D′ and $S_1$′ components. This observation is similar to the results obtained by hot rolling carried out by Maurice and Driver [8,9], Contrepois et al. [10] and Bate et al. [27]. These authors found that at elevated temperature and certain strain levels, there were significant increases of Brass component at the expense of the other β fibre components. It is also noticeable that the maximum texture intensities of pure alloy are higher than those in the 6061 alloy and the nanocomposites at all three orientations and with the additions of SiC particles, the intensities of the major textures become weaker.

The above difference in texture intensities among pure Al, 6061 alloy and nanocomposites is mainly due to the additions of non-deformable SiC particles. For both pure Al and 6061 alloy, during extrusion, the aluminium grains should be elongated along the extrusion direction and a strong

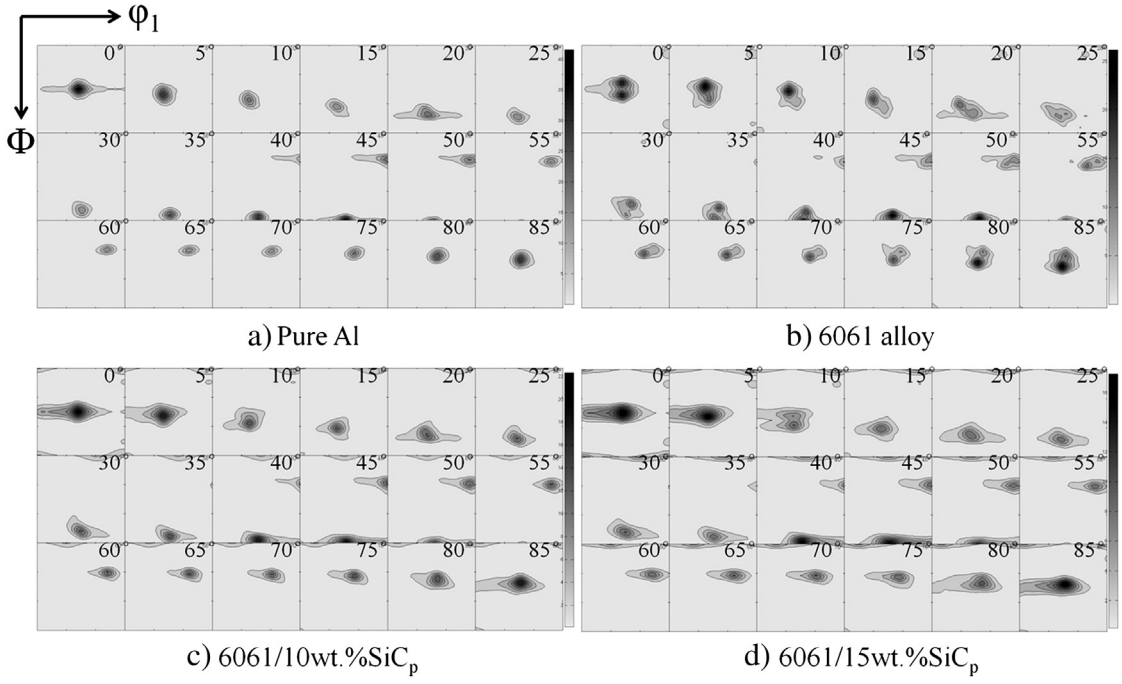


**Figure 2 – ODFs of as-extruded Al, 6061 alloy and 6061/$SiC_p$ nanocomposites in constant $\varphi_2$ sections.**

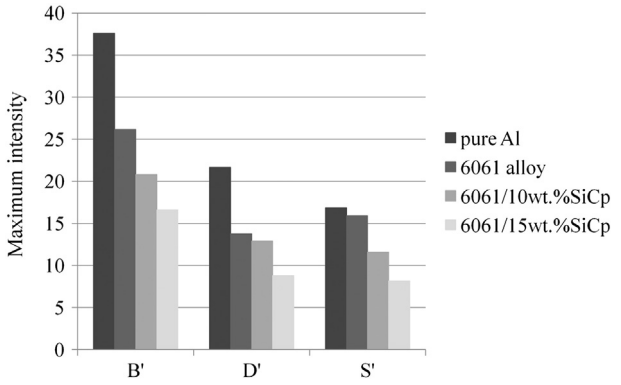


**Figure 3 – Maximum intensity of main texture components near Brass (B′), Dillamore (D′) and $S_1$ (S′) positions.**

deformation texture should develop. For 6061/$SiC_p$ nanocomposites, however, the texture formation would be limited to some extent. As a consequence of the formation of deformation zones around the particles where very high density of dislocations and strong lattice rotations are being built up, grain rotations will be restricted [11,28]. As a result, the grains in these regions cannot rotate to the same orientations as the rest of the matrix, resulting in a weaker deformation texture in the nanocomposites than that of pure Al or 6061 alloy. With the additions of SiC particles, more deformation zones will be formed resulting in more reductions in the intensity of the main textures.

### 3.3. *Crystallographic Texture Study by EBSD*

Fig. 4 shows the inverse pole figure (IPF) maps of as-extruded samples with respect to the normal direction. Each point is painted with a colour according to the crystal orientation. As can be seen in Fig. 4(a) and (b), hot extrusion of pure Al and 6061 alloy has led to the formation of a fibrous deformation structure and elongated grains aligned along the extrusion direction. The scattered IPF data shows a typical β′ fibre texture which is consistent with the ODF results. Images below also show misorientation distributions of Al grain boundaries after extrusion. As can be seen from the misorientation distribution plot, grain boundary populations are not uniformly distributed. Two peaks existed in the range of 0–10° and 50–60°. A large fraction of low-angle (<10°) grain boundaries (25%–30%) was located within the elongated grains. The range of 50–60° corresponds to the grain misorientation between {1 1 0} and {1 1 2} which is consistent with the ODF results that show the texture mainly consists of Brass and Copper orientations.

Fig. 4(c) and (d) shows the Al IPF maps for 6061/$SiC_p$ nanocomposites after extrusion. The EBSD scans were done on both particle free bands and particle rich zones which were separated by dash lines. The EBSD maps show that the Al grain alignment near SiC particles is different from those in the particle free bands. Most of the Al grains in the particle free bands have been rotated to typical Brass or Copper orientations within several degrees' tolerance. Fig. 4(c) and (d) shows {1 1 2} and {1 1 0} planes nearly parallel to the extrusion direction (ED) in the particle free bands, respectively. However, in the particle rich zones, the Al grains are much smaller compared to the grains in the particle free bands. In addition, the orientations of the grains in this region have continuous orientation gradients and are far away from their stable positions near β′ fibre. Most of the grains are equiaxed instead of elongated toward ED. These observations are consistent with ODF results and prove that the additions of SiC particles will lead to local Al grain rotations and weaken the amount of major textures. Compared with the literature with larger SiC particles, in addition to the formation of large deformation zones, lensoid distortions were also found around large SiC particles after plastic deformation, since large particles are highly likely to disturb the slip patterns in the matrix, resulting in a lensoid distortion of the slip planes and sub-structure around the particles [11]. For the present nanocomposites with 500 nm particles, only small volumes of deformation zones associated with local lattice rotations close to the particles were observed and no lensoid distortions have been found.

A closer look of the particle rich zones in Fig. 4(c) and (d) shows the presence of a small amount of the Al grains having {0 0 1} planes nearly parallel to the ED, which is consistent with the ODF results of a weak scattered cube component for 6061/$SiC_p$ nanocomposites. The cube texture is known as the most common recrystallization texture for Al alloys [23]. In order to find out if any dynamic recrystallization happened for 6061/$SiC_p$ nanocomposites during hot extrusion, EBSD scans were performed on the SiC rich areas of as-received and as-extruded 6061/10$SiC_p$ nanocomposites (Fig. 5). From Fig. 5, it is quite clear that the Al matrix was made up of equiaxed grains with high-angle grain boundaries for as-received 6061/10$SiC_p$ sample while after hot extrusion, a fibrous deformation structure with slightly misoriented sub-grains was developed. The EBSD grain size measurement was presented in Fig. 6. The average Al matrix grain size is 1.26 μm and 1.43 μm for as-received and as-extruded 6061/10$SiC_p$ nanocomposites respectively. Dynamic recrystallization and the effect of second phase particles have been extensively studied in Al matrix composites [23,29–32]. It is generally known that large (above 1 μm) widely spaced particles promote rapid nucleation due to the formation of large deformation zones around the particles. While fine closely spaced particles can pin the sub-boundaries and stabilize the sub-structure, nucleation and subsequent growth are retarded and recrystallization is therefore low [23,29,30]. In the present work, the extrusion temperature was very low (375 °C) and the SiC reinforcements have an average diameter of 500 nm which is likely to retard particle stimulated nucleation (PSN). In addition, the comparison of Al grain size between as-received and as-extruded 6061/10$SiC_p$ samples shows no sign of grain refinement due to PSN in the particle rich zones. It is therefore concluded that there is hardly any dynamic recrystallization due to PSN for the nanocomposites during extrusion.

Another possible explanation for the presence of near cube component is the stability of the cube orientation during plastic deformation at high temperatures. Quantitative analyses on hot deformation textures of Al alloys suggest that the cube orientation is stable during large plane strain reductions at high temperatures [8,9,33–35]. Maurice and Driver [8,9,35] have studied and simulated the stability of cube component of Al alloys by channel die compression tests at different

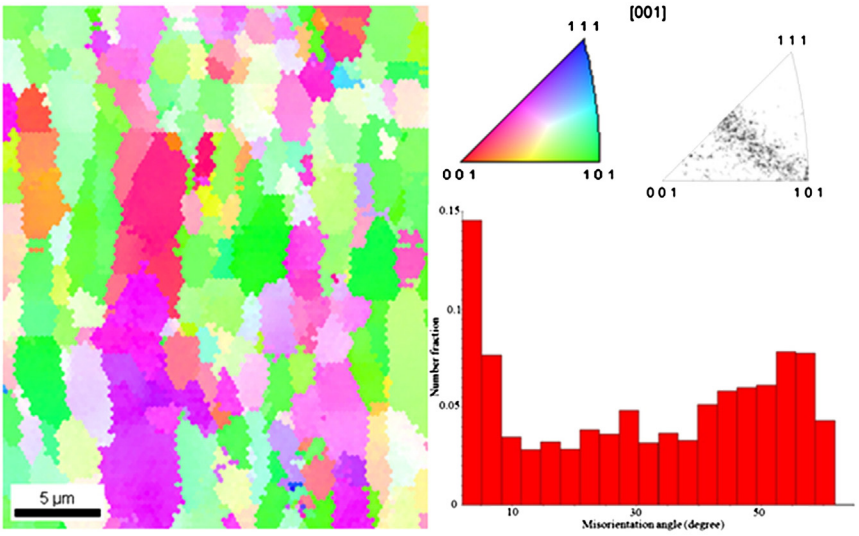


a) Pure Al

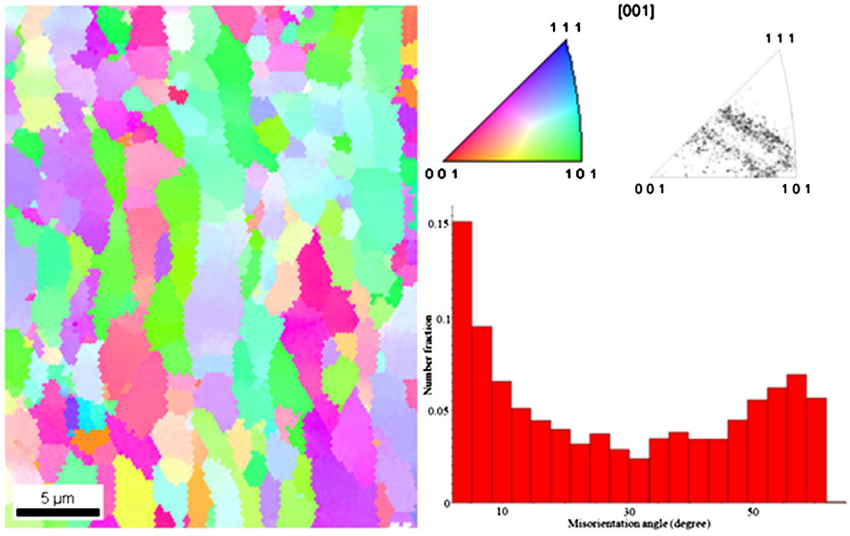


b) 6061 alloy

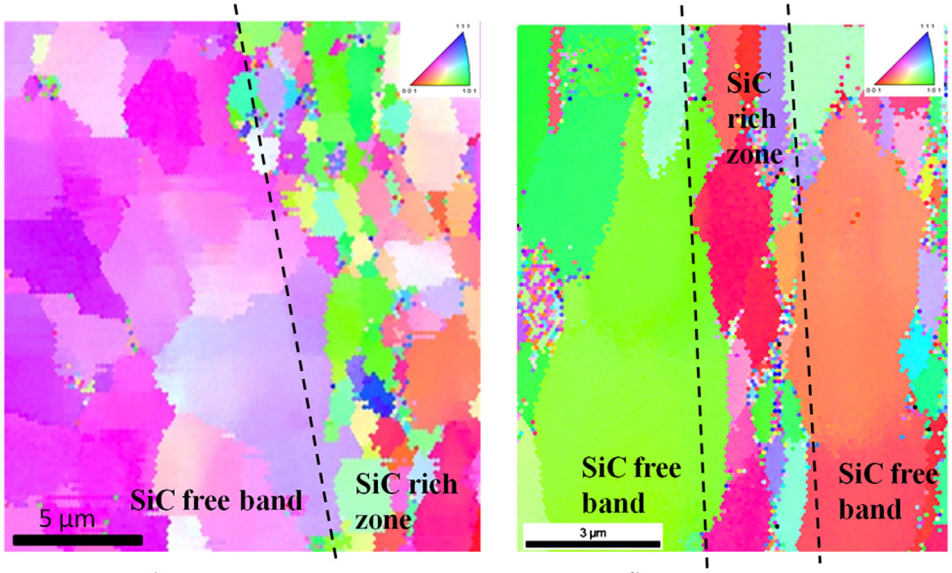


c) 6061/10wt.%$SiC_p$ d) 6061/15wt.%$SiC_p$

**Figure 4 – EBSD maps with IPF and misorientation distribution of as-extruded Al, 6061 alloy and 6061/$SiC_p$ nanocomposites in ED–TD section. (For interpretation of the references to colour in this figure, the reader is referred to the web version of this article.)**

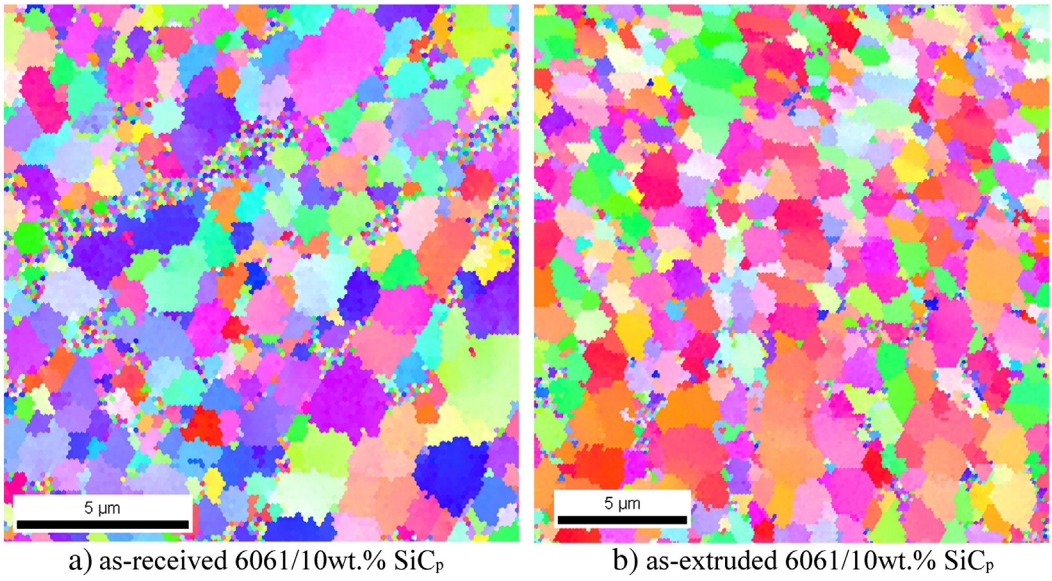


**Figure 5 – EBSD maps with IPF of as-received and as-extruded 6061/10SiC$_p$ nanocomposites in SiC rich zones.**

temperatures. Their results show the appearance of a significant cube component after plane strain compression at 400 °C. It is suggested that at deformation temperatures above 300 °C and high strain rates, the original {1 1 1} <1 1 0> slip systems are replaced by {1 1 0} <1 1 0> type. The onset of {1 1 0} <1 1 0> non-octahedral slip systems stabilizes the cube component which would otherwise rotate towards other more stable orientations. Both experimental results and numerical simulations have verified the active non-octahedral slip systems for cube and near cube orientations and the stability of cube orientation during high temperature deformations. In the as-extruded 6061/SiC$_p$ samples studied in the present work, it is possible that the near cube component is actually the cube orientation in as-received samples which has survived through hot extrusion at 375 °C with just an ER of 6:1.

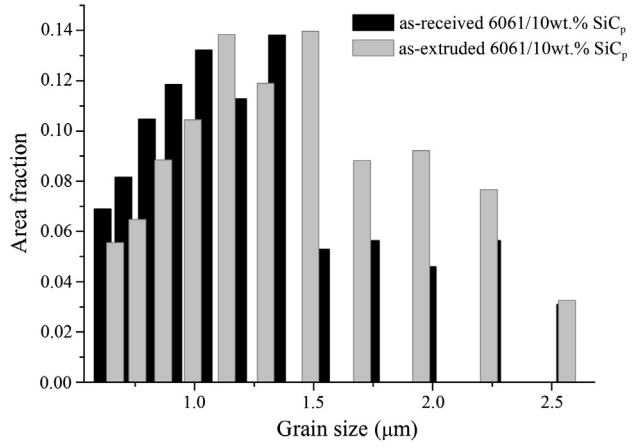


**Figure 6 – Al matrix grain size distribution of as-received and as-extruded 6061/10SiC$_p$ nanocomposites in SiC rich zones.**

## 4. Conclusions

(1) 6061/SiC$_p$ nanocomposites were produced by powder metallurgy using ball milling process followed by extrusion into strip shape. SiC particles showed a non-homogeneous distribution within the matrix due to a combination of the inhomogeneity in as-received materials, lower extrusion ratio and extrusion temperature. Banded structure composed by particle free bands and SiC rich bands was formed in both extruded nanocomposites.

(2) The extrusion texture of 6061/SiC$_p$ nanocomposites consists of three moderate strong texture components, which are {0 10 10} <5 3 3> with a scatter along α fibre, {2 2 5} <10 9 7>, {2 5 10} <10 7 6>, and a weak cube component {0 0 1} <1 0 0>. The three moderate strong texture components are close to the typical β fibre in deformed fcc metals.

(3) Compared to pure Al and 6061 alloy, the intensities of extrusion texture of 6061/SiC$_p$ nanocomposites decrease with increasing volume fractions of SiC particles due to the limited grain rotations around SiC particles.

## Acknowledgements

The authors would like to thank Aerospace Metal Composites Ltd. and Alpoco Ltd. companies for their support of the project. The authors also appreciates the support of Dr. S. Speller for assisting with the texture XRD and Oxford EM group for their help with SEM and EBSD techniques. Dr. M. Galano thanks the RAEng for the support in research through a Research Fellowship. This work was partially supported by the cooperation project PICT-Oxford 2831 and UBACYT 2010/058 grants.

## REFERENCES


[1] Poirier D, Drew RAL, Trudeau ML, Gauvin R. Fabrication and properties of mechanically milled alumina/aluminum nanocomposites. Mater Sci Eng A 2010;527:7605–14.

[2] Rahmani Fard R, Akhlaghi F. Effect of extrusion temperature on the microstructure and porosity of A356–SiCp composites. J Mater Process Technol 2007;187–188:433–6.

[3] Chen MB, Li J, Zhao YM, Yuan H, Liu WC. Comparison of texture evolution between different thickness layers in cold rolled Al–Mg alloy. Mater Charact 2011;62:1188–95.

[4] Kocks UF, Tomé CN, Wenk H-R. Texture and anisotropy: preferred orientations in polycrystals and their effect on materials properties. New York; Cambridge: Cambridge University Press; 1998.

[5] Hirsch J, Lucke K. Mechanism of deformation and development of rolling textures in polycrystalline fcc metals. 1. Description of rolling texture development in homogeneous CuZn alloys. Acta Metall 1988;36:2863–82.

[6] Hirsch J, Lucke K. Mechanism of deformation and development of rolling textures in polycrystalline fcc metals. 2. Simulation and interpretation of experiments on the basis of Taylor-type theories. Acta Metall 1988;36:2883–904.

[7] Hirsch J, Lucke K, Hatherly M. Mechanism of deformation and development of rolling textures in polycrystalline fcc metals. 3. The influence of slip inhomogeneities and twinning. Acta Metall 1988;36:2905–27.

[8] Maurice C, Driver JH. Hot rolling textures of fcc metals—part I: experimental results on Al single and polycrystals. Acta Mater 1997;45:4627–38.

[9] Maurice C, Driver JH. Hot rolling textures of fcc metals—part II: numerical simulations. Acta Mater 1997;45:4639–49.

[10] Contrepois Q, Maurice C, Driver JH. Hot rolling textures of Al–Cu–Li and Al–Zn–Mg–Cu aeronautical alloys: experiments and simulations to high strains. Mater Sci Eng A 2010;527:7305–12.

[11] Humphreys FJ, Miller WS, Djazeb MR. Microstructural development during thermomechanical processing of particulate metal–matrix composites. Mater Sci Technol 1990;6:1157–66.

[12] Jensen DJ, Hansen N, Humphreys FJ. Effect of metallurgical parameters on the textural development in fcc metals and alloys. Proceedings of ICOTOM 8 International Conference on Textures of Materials; 1987. p. 431–44.

[13] Shahani RA, Clyne TW. The effect of reinforcement shape on recrystallization in MMCs. Proceedings of the 12th Risø International Symposium on, Materials Science; 1991. p. 655–60.

[14] Ramesh CS, Keshavamurthy R, Koppad PG, Kashyap KT. Role of particle stimulated nucleation in recrystallization of hot extruded Al 6061/SiCp composites. Trans Nonferrous Met Soc China 2013;23:53–8.

[15] He CL, Wang JM, Cai QK. Effects of particle size and volume fraction on extrusion texture of SiCp/Al metal matrix composites. Adv Eng Mater 2011;194–196:1437–41 [Pts 1–3].

[16] Hielscher R, Schaeben H. A novel pole figure inversion method: specification of the MTEX algorithm. J Appl Crystallogr 2008;41:1024–37.

[17] Ocelík V, Vreeling JA, De Hosson JTM. EBSP study of reaction zone in SiC/Al metal matrix composite prepared by laser melt injection. J Mater Sci 2001;36:4845–9.

[18] Lee JC, Subramanian KN. Effect of cold-rolling on the tensile properties of ($Al_2O_3$)P/Al composites. Mater Sci Eng A 1992;159:43–50.

[19] Borrego A, Fernandez R, Cristina MD, Ibanez J, Gonzalez-Doncel G. Influence of extrusion temperature on the microstructure and the texture of 6061Al–15 vol.% SICwPM composites. Compos Sci Technol 2002;62:731–42.

[20] Sun YP, Yan HG, Su B, Jin L, He JM. Microstructure and mechanical properties of spray deposition Al/SiCp composite after hot extrusion. J Mater Eng Perform 2011;20:1697–702.

[21] Wang XJ, Xu L, Hu XS, Nie KB, Deng KK, Wu K, et al. Influences of extrusion parameters on microstructure and mechanical properties of particulate reinforced magnesium matrix composites. Mater Sci Eng A 2011;528:6387–92.

[22] Wang ZW, Song M, Sun C, Xiao DH, He YH. Effect of extrusion and particle volume fraction on the mechanical properties of SiC reinforced Al–Cu alloy composites. Mater Sci Eng A 2010;527:6537–42.

[23] Humphreys FJ, Hatherly M. Recrystallization and related annealing phenomena. Oxford: Pergamon; 1995.

[24] Poudens A, Bacroix B, Bretheau T. Influence of microstructures and particle concentrations on the development of extrusion textures in metal–matrix composites. Mater Sci Eng A 1995;196:219–28.

[25] Inoue H. Texture of extruded aluminum alloys. Keikinzoku/J Jpn Inst Light Met 2002;52:524–9.

[26] Chen LQ, Kanetake N. Hot-extruded and cold-rolled textures of the matrix aluminum in deformation processed two-phase Nb/Al metal–metal composites. Textures Microstruct 2003;35:273–82.

[27] Bate PS, Huang Y, Humphreys FJ. Development of the “brass” texture component during the hot deformation of Al–6Cu–0.4Zr. Acta Mater 2004;52:4281–9.

[28] Engler O, Kong XW, Yang P. Influence of particle stimulated nucleation on the recrystallization textures in cold deformed Al-alloys. 1. Experimental observations. Scr Mater 1997;37:1665–74.

[29] Shahani RA, Clyne TW. Recrystallization in fibrous and particulate metal matrix composites. Mater Sci Eng A 1991;135:281–5.

[30] Doherty RD, Hughes DA, Humphreys FJ, Jonas JJ, Jensen DJ, Kassner ME, et al. Current issues in recrystallization: a review. Mater Sci Eng A 1997;238:219–74.

[31] Zhong WM, Goiffon E, LEsperance G, Suery M, Blandin JJ. Effect of thermomechanical processing on the microstructure and mechanical properties of Al–Mg (5083)/SiCp and Al–Mg (5083)/Al(2)O(3)p composites. 1. Dynamic recrystallization of the composites. Mater Sci Eng A 1996;214:84–92.

[32] Ko BC, Park GS, Yoo YC. The effects of SiC particle volume fraction on the microstructure and hot workability of SiCp/AA 2024 composites. J Mater Process Technol 1999;95:210–5.

[33] Daaland O, Nes E. Origin of cube texture during hot rolling of commercial Al–Mn–Mg alloys. Acta Mater 1996;44:1389–411.

[34] Panchanadeeswaran S, Field DP. Texture evolution during plane-strain deformation of aluminum. Acta Metall Mater 1995;43:1683–92.

[35] Maurice C, Piot D, Klocker H, Driver JH. Hot plane strain compression testing of aluminum alloys by channel-die compression. Metall Mater Trans A 2005;36A:1039–47.